JOURNAL OF Materials CHEMISTRY

A stable and flexible dianion: 2-dicyanomethylene-1,1,3,4,5,5-hexacyanopentenediide ($DHCP^{2-}$), and its complex formation†

Gunzi Saito,*[a] Shuichi Sekizaki,[a] Akihiko Konsha,[a] Hideki Yamochi,[a,b] Kiyoshi Matsumoto,[c] Masami Kusunoki[d] and Ken-ichi Sakaguchi[d]

[a]*Division of Chemistry, Graduate School of Science, Kyoto University, Kyoto 606-8502, Japan. E-mail: saito@kuchem.kyoto-u.ac.jp*
[b]*CREST, Japan Science and Technology Corporation (JST), Japan*
[c]*Graduate School of Human and Environmental Studies, Kyoto University, Kyoto 606-8501, Japan*
[d]*Institute for Protein Research, Osaka University, Suita, Osaka 565-0871, Japan*

Received 7th August 2000, Accepted 13th October 2000
First published as an Advance Article on the web 7th December 2000

2-Dicyanomethylene-1,1,3,4,5,5-hexacyanopentene (DHCP) dianion, which had been reported as 2,3-bis(dicyanomethyl)-1,1,4,**4-t**etracyanobutadiene, was synthesized as a tetraalkylammonium salt from hexacyanobutadiene. The crystal structures of tetraalkylammonium (alkyl: methyl, ethyl), tetrathiafulvalene (TTF) and bisethylenedithio–TTF (BEDT–TTF or ET) salts were solved. Possible reaction processes to give DHCP were deduced based on its molecular structure. Fourteen solid charge transfer complexes, seven of which were highly conductive, were prepared with mainly TTF derivatives as electron donor. ET afforded two metallic complexes, one of which (**ET1**) showed a metal–insulator transition at 180 K and the other (**ET2**) retained metallic behavior down to 1.3 K. BEDO–TTF complex was metallic down to 4.2 K. The crystal, electronic and band structures and EPR parameters of **ET1** and **ET2** were studied. Both **ET1** and **ET2** have a β″-type packing mode with significantly different mutual orientation between ET and DHCP molecules. The polymorphism is relevant to both different conformations of DHCP; *cis* and *trans*, which demonstrate the flexibility of the molecular shape and conformation, and intermolecular atomic contacts between ET and DHCP molecules.

1 Introduction

The reaction properties of a variety of polycyanocarbons and their derivatives have attracted the interest of chemists.[1] The interest for practical applications was also aroused for use as deeply colored dyes,[1b,2] catalysts[3] and nonlinear optical materials.[4] Among them, formation of highly conductive charge transfer (CT) complexes[5] and ferro- or antiferromagnetic CT complexes[6] have been most intensively investigated with respect to their properties as electron acceptors or anions by both chemists and physicists. Recently, polycyanocarbons have been examined as coordinated ligands to metals and as the basis for supramolecular frameworks.[7] The highest T_c organic superconductors of bisethylenedithio–tetrathiafulvalene (BEDT–TTF or ET), κ-$(ET)_2[Cu\{N(CN)_2\}X]$ (X = Br, Cl, CN),[8] and new exotic organic magnets have been discovered.[9]

In 1964, Webster synthesized some polycyanocarbons with strong electron accepting abilities, these included hexacyanobutadiene (HCBD, **1** in Fig. 1), heptacyanopentadiene (HPCPD, **2**) and 2,3-bis(dicyanomethyl)-1,1,4,4-tetracyanobutadiene (BDCTCB, **3**).[10] The compounds **2** and **3** were described as a monoanion and a dianion, respectively. The chemical structure of **3** was postulated based on the absorption spectra, elemental analysis and reaction mechanism.

The molecule **3** has eight cyano groups on the periphery of the molecule and is thought to be a stable and polarizable symmetric dianion with high flexibility around the central carbon–carbon single bond. These molecular features are ideal factors, though its bulkiness is not, for obtaining highly

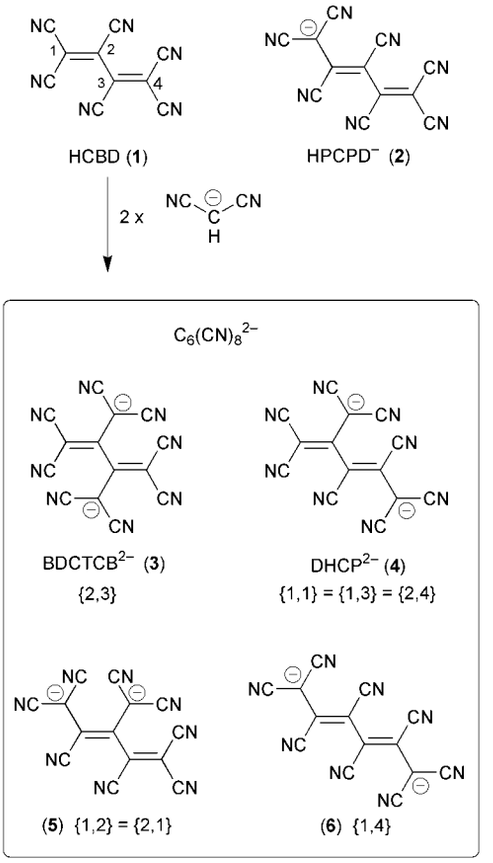

Fig. 1 HCBD (**1**), HPCPD (**2**) and four possible octacyano compounds **3**–**6** with C_6 skeletons: $C_6(CN)_8$, derived by the replacement of two cyano groups of HCBD by two dicyanomethyl groups.

†Atomic structures of **TTF**, **ET1** and **ET2** are available as supplementary data. For direct elctronic access see http://www.rsc.org/suppdata/jm/b0/b006426m/

 DOI: 10.1039/b006426m

This journal is © The Royal Society of Chemistry 2001

conductive CT complexes of a radical cation salt using **3** as a counter anion. As a part of our continuing investigation on the CT complexes based on organic anions or strong acceptor molecules,[11] we report here the detailed results of a dianion molecule; 2-dicyanomethyl-1,1,3,4,5,5-hexacyanopentadiene (DHCP, **4** in Fig. 1), which Webster reported as **3**. Both **3** and **4** are among the octacyano compounds having eight cyano groups on the periphery of the C_6 skeleton: $C_6(CN)_8$(Fig. 1, **3**–**6**), which have been briefly reported in the previous paper.[12]

2 Experimental

2.1 Synthesis

The synthetic scheme of DHCP (**4**) from HCBD (**1**) is almost the same as that for **3** reported by Webster.[10] Into a cooled suspension of 7.5 g of sodium hydride (60% in oil, 187 mmol) in 50 mL of 1,2-dimethoxyethane (DME), a solution of 1.26 g (19.1 mmol) of malononitrile in 25 mL of DME (NaH : malononitrile $\approx$ 10 : 1) was added dropwise at 5 °C and the reaction mixture was cooled below −50 °C. Into this cooled mixture, 1.92 g (9.40 mmol) of **1** dissolved in 25 mL of dry acetonitrile under nitrogen was added dropwise for 1.5 h then warmed to room temperature. By addition of 500 mL of ether into the solution, brownish gummy solids were isolated. These solids were treated as reported by Webster to give $(TEA)_2$**4** by using tetraethylammonium (TEA) bromide, red solid 1.04 g (1.92 mmol, 20.4%). Tetramethylammonium (TMA) or tetra-*n*-propylammonium (TPA) bromide gave $(TMA)_2$**4** or $(TPA)_2$**4**, respectively. Use of a smaller excess of sodium hydride such as a molar ratio of NaH : malononitrile = 1 : 1 (as used by Webster) results in a poorer yield of the product (6.3%).

Elemental analysis of $(TEA)_2$ **4** satisfies $(TEA)_2C_6(CN)_8$ (calc. for $C_{30}H_{40}N_{10}$: C 66.64, H 7.46, N, 25.90; obs. C 66.86, H 7.63, N 25.87%). The comparison of melting point, IR and UV–Vis spectra and elemental analysis of $(TEA)_2$**4** indicates that the compound synthesized here is identical to that reported for **3**.[10,12,13] The corresponding data for $(TMA)_2$**4** and $(TPA)_2$**4** are reported in reference 12.

$(TEA)_2$**4** exhibited only one oxidation peak potential at +1.3 V *vs.* SCE (saturated calomel electrode) or +1.22 V *vs.* Ag/AgCl in the cyclic voltammogram[14] indicating that the dianion state of **4** is very stable.

2.2 Preparation of charge transfer complexes

Solid CT complexes were prepared by the methathesis or the electrocrystallization method. Table 1 summarizes the results for typical cases. Hereafter, the complexes are represented by the name in the last column in Table 1.

The methathesis method was applied only for the tetrathiafulvalene (TTF) complex. The acetonitrile solutions of $(TTF)_3(BF_4)_2$ and $(TEA)_2$**4** were combined at room temperature and concentrated to give CT complex (block shape: **TTF**) together with $(TTF)_3(BF_4)_2$ (long plate). They were washed with acetonitrile then vacuum dried overnight. The single crystals of **TTF** were separated under a microscope.

The electrocrystallization method was applied for the electron donor molecules in Fig. 2 (reference 15) using three kinds of solvents for every case; tetrahydrofuran (THF), 1,1,2-trichloroethane (TCE) and benzonitrile (PhCN), in an H-shaped cell of 20 mL under a constant current of 0.2–2.0 μA for 10–60 days. The concentration of the electrolyte $(TEA)_2$ **4** is about 2.3×10^{-3} mol L^{-1}.

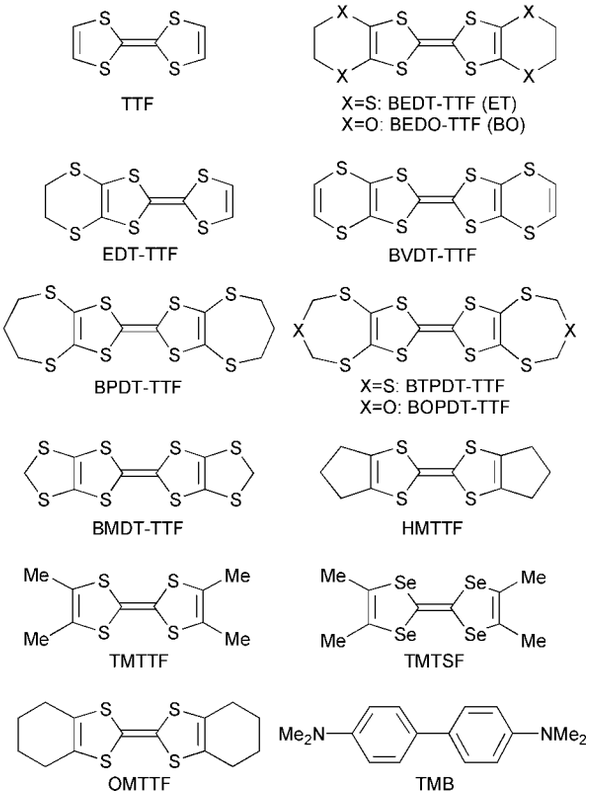

Fig. 2 Donor molecules: TTF, BEDT–TTF (ET), BEDO–TTF (BO), EDT–TTF, BVDT–TTF, BPDT–TTF, BTPDT–TTF, BOPDT–TTF, BMDT–TTF, HMTTF, TMTTF, TMTSF, OMTTF and TMB.

Table 1 Characteristics of charge transfer complexes of $DHCP^{2-}$

Donor[a]	Solvent[b]	Appearance	Conductivity[c]		Optical bands[d]/10^3 cm^{-1}				Sample name
			σ_{RT}/S cm^{-1}		A	B	C	D	
BEDT–TTF	THF	Black plate	$10–10^2$	T_{MI} = 180 K	3.5–4.1	—	10.6	16.5	**ET1**
BEDT–TTF	THF	Black needle	$10–10^2$	Metal > 1.3 K	3.4	—	10.6	16.3	**ET2**
BEDO–TTF	THF	Black plate	10^2	Metal > 4.2	2.7–3.0	—	13.0	17.4	**BO**
BMDT–TTF	THF	Brown plate	insulator		—	—	11.3	—	**MT1**
BMDT–TTF	TCE	Brown wool	5×10^{-1}	ε_a = 25 meV	3.8	8.4	—	—	**MT2**
BPDT–TTF	TCE	Black plate	3×10^{-3}	ε_a = 70 meV	3.6	—	13.7	17.4	**PT**
EDT–TTF	TCE	Black plate	10^2	Metal–semicon.	3.9	—	13.9	—	**EDT**
BVDT–TTF	TCE	Brown needle	10^2	Metal–semicon.	3.2	—	10.7	16.4	**VT**
BOPDT–TTF	TCE	Black needle	1	ε_a = 50 meV	4.0	—	14.3	16.8	**BOP**
TTF	CH_3CN	Black block	10^{-7}		—	12.3	—	19.2	**TTF**
TMTTF	THF	Black plate	10^{-10}		—	11.5	—	17.2	**TMTTF**
TMTSF	THF	Brown plate	10^{-5}		—	8.8	14.9		**TMTSF**
HMTTF	THF	Black plate	Insulator		—	10.3	15.9		**HM**
TMB	THF	Purple powder	Insulator		—	8.0	14.0		**TMB**

[a]See Fig. 2. [b]THF: tetrahydrofuran, TCE: 1,1,2-trichloroethane. [c]σ_{RT}: room temperature conductivity, ε_a: activation energy for conduction. [d]KBr pellet sample. As for bands A–D, see text.

Optical measurements revealed that there were two kinds of ET complexes (**ET1** (minor product), **ET2** (major product)) and BMDT–TTF complexes (**MT1**, **MT2**). For each of the other donors, as far as the optical results were concerned, only one kind of complex was obtained whatever the solvents were. Plate-like crystals (**ET1**) and needle-like crystals (**ET2**) were obtained from THF. Plate-like crystals from benzonitrile and wool-like crystals from TCE were identified to be similar to **ET1** and **ET2**, respectively. The electrocrystallization using TTF, OMTTF and BTPDT–TTF afforded no solid under our reaction conditions. The yield of the CT complex was very low for the purpose of determining the stoichiometry by elemental analysis. Only a few complexes in Table 1 were examined with regard to their stoichiometries by crystallographic analysis together with density measurements.

2.3 Measurements

DC conductivities of the CT complexes were measured by a standard four- or two-probe technique using gold wires of 10 μm diameters with gold paste (Tokuriki, 8560-1A) or carbon paste (Ladd Research Ind.). The results are summarized in Table 1.

IR spectra (400–7800 cm^{-1}) and UV–Vis spectra (240–2600 nm) were measured by Perkin-Elmer 1600 Series FT-IR (resolution 4 cm^{-1}) and Shimadzu UV-3100, respectively, on KBr pellet samples. The main peak energies in UV–Vis–NIR spectra are summarized in Table 1. They also show two additional peaks at $22–23\times10^3$ and $29.5–30.5\times10^3$ cm^{-1} in KBr ($\lambda_{max}=329$, 420 nm in acetonitrile) which are ascribed to $\mathbf{4}^{2-}$.

EPR spectra were measured on a JEOL JES-RE2X X band EPR spectrometer equipped with the temperature controller Oxford EPR-900 cryostat.

X-Ray diffraction data were collected on automatic four circle diffractometers (Rigaku AFC-4 or AFC-5) with graphite monochromated Mo-Kα radiation at room temperature. Crystal structures of the complexes were solved by direct method (SIR92) and refined by full matrix least-squares method on F^2 (SHELXL-93).[16]‡

Band structures of **ET1** and **ET2** were calculated based on the crystal structures by extended Hückel tight-binding method with single-ζ parameters including d-orbitals of sulfur atoms.[17] Taking into account the disorder of the terminal ethylene groups of ET molecules for both **ET1** and **ET2**, we performed the calculations on eight different configurations and the calculated band structures were nearly identical among them. The value of the overlap integrals for the band calculations of **ET1** and **ET2**, and the calculated band structure of **ET1** using double-ζ Slater parameters are provided as supplementary data.†

3 Results and discussion

3.1 Molecular structure, reaction process and flexibility of $\mathbf{4}^{2-}$

Fig. 1 summarizes the four possible structures of $C_6(CN)_8$ (**3**–**6**) produced by the replacement of two cyano groups of HCBD (**1**) by two dicyanomethyl groups. Compound **3** is a product of successive substitution firstly at the 2- and then at the 3-positions of **1**, which is denoted by {2,3}. The {2,3} has two carbon atoms which have two dicyanomethyl groups. The compound **4** is {1,1}, {1,3} or {2,4}, all of which are identical and have both one carbon atom bearing two dicyanomethyl groups and the other one bearing one dicyanomethyl group. The molecule **5** represents {1,2} or {2,1}, which has three carbon atoms with one dicyanomethyl group. The last one is **6**, {1,4}, which has two carbon atoms with one dicyanomethyl group. The seven combinations; {1,1}, {1,2}, {1,3}, {1,4}, {2,1}, {2,3} and {2,4}, cover all the processes to obtain $C_6(CN)_8$ by successive substitution reactions.

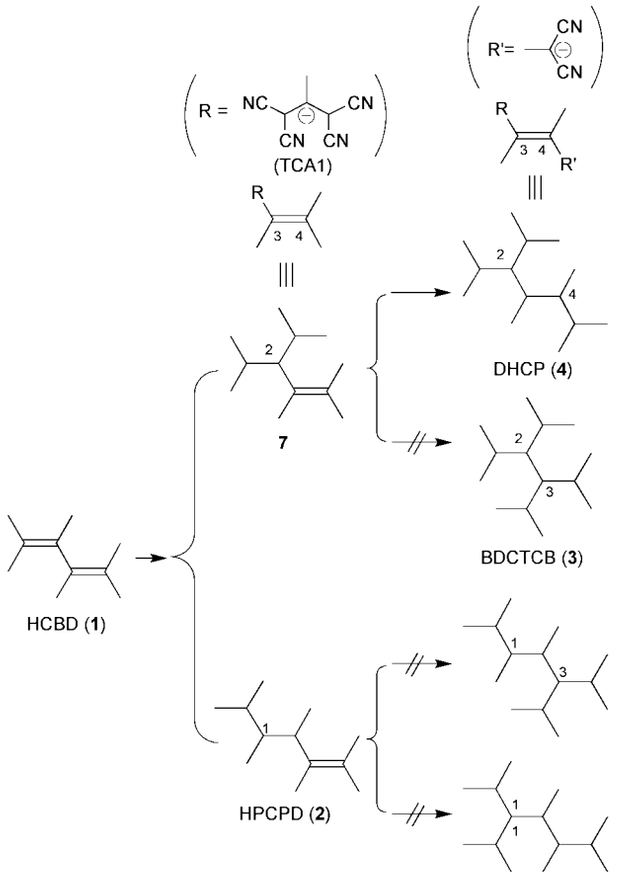

Fig. 3 Possible reaction mechanism to give DHCP. Cyano groups are indicated as sticks.

Fig. 3 shows the possible reaction process of $C_6(CN)_8$. The formation of **3** was deduced by Webster based on the following observations;[10] (1) the compound is a double substitution product (a dicyanomethyl group replaces a CN group) of **1**, (2) the product shows a similar UV–Vis spectrum in solution to that of the pentacyanoallyl anion (PCA^- (**8**), Fig. 4, $\lambda_{max}=412$ nm) and (3) the product is not available from an equimolar reaction of heptacyanopentadiene anion ($HPCPD^-$, **2**) and malononitrile anion. Thus the molecular structure {2,3} was postulated, which would be constructed by a bond formation of two 1,1,3,3-tetracyanoallyl molecules (TCA1 (**9**), Fig. 4) at each 2-position. The item (3) observed by Webster suggests that the production of {1,*n*} ($n=1–4$) is not probable.

We identified the structure of the reaction product by the crystal structure analysis of $(TMA)_2\mathbf{4}$, $(TEA)_2\mathbf{4}$ and $(TTF)_2\mathbf{4}(CH_3CN)$.[12] As a consequence, it is concluded that the product is 2-dicyanomethyl-1,1,3,4,5,5-hexacyanopentadiene (DHCP) which corresponds to {1,1}, {1,3} or {2,4} but not to {2,3}. Thus only **4** is produced by the successive substitutions at the 2- and 4-positions of **1**. The molecular structure of DHCP is equivalent to a combination of TCA1 (**9**) and TCA2 (**10**, Fig. 4) at the 2- and 3-positions, respectively.

The reaction seems to occur between a malononitrile anion and **7**, a monosubstituted tetracyanoethylene (TCNE) by TCA1, in Fig. 3. The substitution of the dicyanomethyl group for the second CN group occurs at the 4-position of **7** to give the {2,4}, and not at the sterically crowded 3-position which gives the {2,3}.

‡CCDC reference number 1145/255. See http://www.rsc.org/suppdata/jm/b0/b006426m/ for crystallographic files in .cif format.

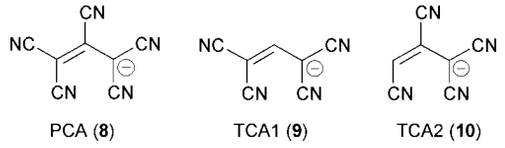

Fig. 4 Pentacyanoallyl anion (PCA), 1,1,3,3-tetracyanoallyl anion (TCA1) and 1,1,2,3-tetracyanoallyl anion (TCA2).

Fig. 5 shows the molecular structures of DHCP in the TMA, TEA and TTF salts[12,18] and the schematic figure of DHCP. Only the *cis*-like conformation (Fig. 5f) is observed in the TMA and TEA salts (Fig. 5a, b). However, in **TTF** (Fig. 5c), a positional disorder is seen at the right half; TCA2 part of DHCP. All atoms in the TCA2 part are almost coplanar. The site occupancies of *trans*-like (shaded atoms and solid bonds) and *cis*-like structures (unshaded atoms and open bonds) are 0.58(1) and 0.42(1), respectively. This disorder is caused by the rotational flexibility of the C4–C5 bond of DHCP. Similar disorders have been reported in PCA^- (**8**, Fig. 4).[19] It is also noticed that the DHCP molecule is non-planar and flexible in its shape and conformation. The feature is clearly observed by examination of the dihedral angle (φ, see Fig. 5d) between the terminal bis(dicyanomethyl)methylide group (TCA1 part) linked to C4 and the rest, the TCA2 part of DHCP. The φ value varies from 69.8° for **TTF** to 55.9° for the TMA salt (Table 2).

The TCA1 part linked to C4 also presents the flexible feature. The dihedral angles (ϕ, Fig. 5d) made by planes composed of carbon atoms of C1–C2–C3 and two dicyanomethyl groups attached to C1 varies from 0.9 and 4.0° for **TTF** to 15.2 and 6.9° for the TEA salt for the dicyanomethylene groups N1≡C7–C2–C8≡N2 and N3≡C9–C3–C10≡N4, respectively (Table 2).

As a summary, it should be emphasized that the DHCP molecule has an ability to modify its shape and conformation to some extent depending on the shape and size of counter cation molecule and surrounding circumstances (*vide infra*).

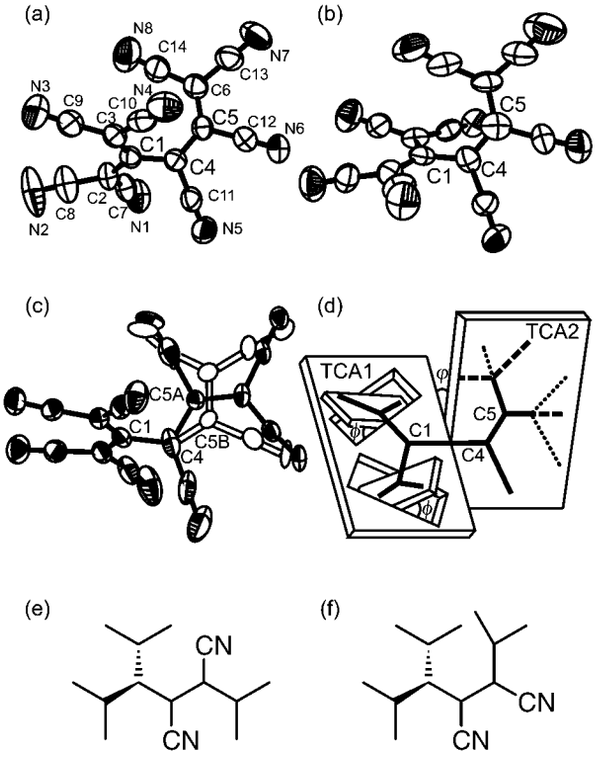

Fig. 5 Molecular structures of $DHCP^{2-}$ in the TMA(a), TEA(b) and TTF(c) salts. In $(TTF)_2(DHCP)(CH_3CN)$ (**TTF**), positional disorder is observed with site occupancy factors of 0.58 (shaded atoms and solid bonds) and 0.42 (unshaded atoms and open bonds). The schematic figure (d) clarifies the dihedral angles ϕ and φ. Dotted lines and dashed lines correspond to *trans*- and *cis*- like structure, respectively. (e) and (f) also show *trans*- and *cis*-like conformations, respectively.

Table 2 Conformation of TCA2 and dihedral angles ϕ and φ in $DHCP^{2-}$

Cation	Conformation	φ	ϕ_1	ϕ_2
TMA	*cis*	55.9	12.2	14.1
TEA	*cis*	64.1	15.2	6.9
TTF (**TTF**)	*trans*/*cis*	69.1/69.8	0.9	4.0
ET (**ET1**)	*cis*	65.8	13.3	14.6
ET (**ET2**)	*trans*	53.6	17.7	20.2

3.2 Absorption spectra of charge transfer complexes of DHCP

The fifth column in Table 1 summarizes the optical absorption peak energies of the typical samples. According to the optical spectra, the samples of ET complexes are divided into two, though both exhibited very similar spectra to each other (*a, b* in Fig. 6). The lowest energy absorption band appears at 3.4–4.1×10^3 cm^{-1} (denoted band A), which indicates both the partial CT state and the segregated manner of the ET molecules in the solid. The existence of band A also suggests the highly conductive nature of the complex, provided that the complex does not have both charge separation and lattice distortion. The next band at 10.6×10^3 cm^{-1} and a very weak shoulder-like band at $16.3–16.5 \times 10^3$ cm^{-1} are ascribed to the intramolecular transition from second HOMO to HOMO (denoted band C) and HOMO to LUMO (denoted band D) of $ET^{+\cdot}$ molecule,[20] respectively. Band A of the sample **ET2** is more intense than band C. On the other hand, bands A and C are comparable in their intensities in the sample **ET1**. Accordingly it is very likely that **ET1** is different from **ET2**. This is consistent with the conductivity and structural results as described below.

In **BO** (*c* in Fig. 6) a very intense band A is observed at 2.7–3.0×10^3 cm^{-1} followed by a weak band C at 12.4–13.0×10^3 cm^{-1} and a very weak band D at 16.8–17.4×10^3 cm^{-1}. The coexistence of bands A and C are also noticed in highly conductive **EDT** (*d*) and **VT** (*e*). Semiconductors **PT** (*f*) and **BOP** (*g*) have the same features. On the other hand, a semiconductor **MT2** (*h*) exhibits both bands A (3.8×10^3 cm^{-1}) and B (8.4×10^3 cm^{-1}), which is not observed in curves *a–g* in Fig. 6, indicating that the degree of CT is more than 0.5.

However, the following samples do not exhibit band A; **TTF**, **MT1**, **TMTTF**, **TMTSF**, **HM** and **TMB**. The lack of band A is consistent with the insulating nature of these compounds. As

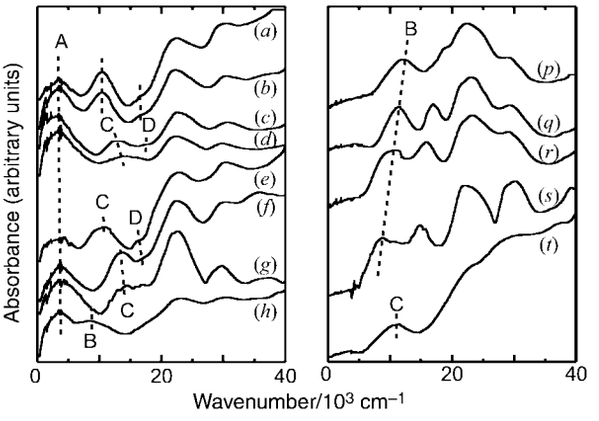

Fig. 6 Absorption spectra in KBr. Left: conducting solid complexes ((*a*):**ET1**, (*b*):**ET2**, (*c*):**BO**, (*d*):**EDT**, (*e*):**VT**, (*f*):**PT**, (*g*):**BOP**, (*h*):**MT2**. Right: insulating solid complexes ((*p*):**TTF**, (*q*):**TMTTF**, (*r*):**HM**, (*s*):**TMTSF**, (*t*):**MT1** For bands A, B, C and D, see text.

shown in Fig. 6 (right), the lowest optical transition energies of them are 12.3 (**TTF** (*p*)), 11.5 (**TMTTF** (*q*)), 10.3 (**HM** (*r*)) and 8.8×10^3 cm^{-1} (**TMTSF** (*s*)) and are ascribed to the optical transition between the donor cation radical molecules (denoted band B) confirming the presence of the segregated columns of donor molecules. In the case of **MT1** (*t*), only band C (11.3×10^3 cm^{-1}) appears.

3.3 Electrical conductivity

The conduction characteristics are summarized in the fourth column in Table 1 for the typical samples. Even though **ET1** and **ET2** exhibit almost the same UV–Vis–NIR spectra, their conducting behavior is different to each other. **ET1** is highly conductive with room temperature (RT) conductivity $\sigma_{RT} = 10$–100 S cm^{-1} within a plane ($=\sigma_{//}$). It shows a slight decrease of resistivity down to 180 K followed by a rapid increase (Fig. 7a). The conduction anisotropy in the largest plane of the plate-like crystal ($0.8 \times 0.5 \times 0.2$ mm^3) indicates an almost isotropic nature, while the conductivity normal to the conducting plane is *ca.* $\sigma_{\perp} = 10^{-3}$ S cm^{-1}. So the material **ET1** is an excellent two-dimensional (2D) conductor with $\sigma_{//}/\sigma_{\perp} = 10^4 - 10^5$. The magnitude of anisotropy is comparable to those of typical 2D-conductors α-$(ET)_2MHg(SCN)_4$(M = K, NH_4) ($\sigma_{//}/\sigma_{\perp} \geqslant 10^3 - 10^6$)[21] indicating that the conducting 2D ET layers are well shielded by an insulating anion layer composed of $DHCP^{2-}$ and THF (*vide infra*).

ET2 is metallic down to 1.3 K with $\sigma_{RT} = 10$–100 S cm^{-1}. Fig. 7b shows temperature dependence of the fresh sample of **ET2**. No anisotropic data are available due to the size of the needle-like crystals ($1.2 \times 0.06 \times 0.02$ mm^3). Occasionally semiconductive behavior was observed down to 200 K followed by metallic behavior. Furthermore some **ET2** samples exhibit almost flat temperature dependence down to 100 K followed by semiconductive behavior (Fig. 7c). The varied temperature dependence is also observed in **ET1** samples, one of which exhibits semiconductive behavior with $\sigma_{RT} = 1.4$ S cm^{-1} and activation energy of $\varepsilon_a = 218$ meV. Such varied temperature dependence of **ET1** and **ET2** was observed on old samples and is possibly ascribed to the combination of the loss of volatile solvent included in the crystals, the stoichiometries of which are $(ET)_4(DHCP)(THF)_x$ ($x \approx 2$), and the flexible conformation of DHCP which may occupy the void generated by the loss of the solvent.

Even though the stoichiometries of complexes are not clarified for **VT** and **EDT** samples, the similar varied temperature dependencies of resistivity; *i.e.* from metal to semiconductor, are observed in these samples.

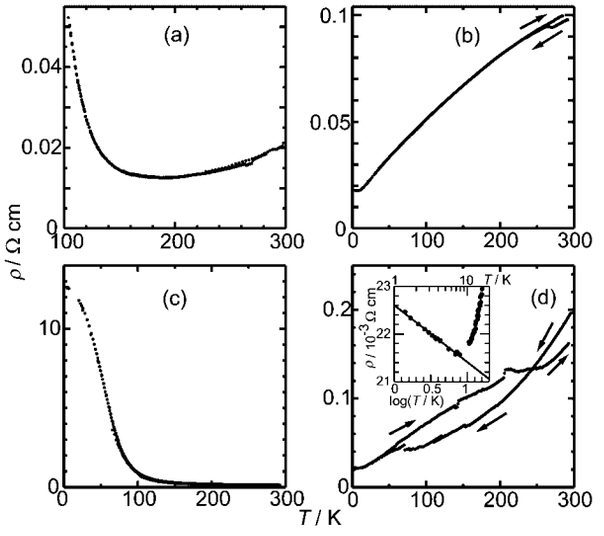

Fig. 7 Temperature dependence of resistivity (a): **ET1**, (b): the best sample of **ET2**, (c): other sample of **ET2**, (d): **BO**; inset: low temperature region of **BO** (log*T* plot).

BO is metallic down to 8 K followed by a slight increase of resistivity (Fig. 7d). The resistivity at 4.2 K is still about one tenth of that at RT. The resistivity below 8 K exhibits log*T* dependence (inset of Fig. 7d) suggesting weak localization of 2D conduction electrons owing to disorder.[22]

The samples of **MT2**, **PT** and **BOP** are semiconductive with the σ_{RT} and ε_a values cited in Table 1, and they do not show varied temperature dependence.

The other complexes in Table 1 are insulators with σ_{RT} less than 10^{-5} S cm^{-1}, consistent with loss of band A in the UV–Vis–NIR spectra. It is noteworthy that the donor molecules in most of the insulating complexes are somewhat smaller than those in the conducting complexes and do not have the additional outer alkylchalcogeno group to TTF moiety. These facts show the importance of the chalcogen–chalcogen intermolecular atomic contacts, which may increase the electronic dimensionality of the complexes, to reveal significant electric conductivity in the DHCP complexes.

Ideally, to understand the physical properties of the complexes, the crystal structures are needed. However, only a few complexes had crystal quality suitable for structure determination. In the following, the crystal structure of the insulating salt (**TTF**) and the two conducting salts (**ET1** and **ET2**) are described.

3.4 Crystal structure of $(TTF)_2(DHCP)(CH_3CN)$

This compound is an insulator since the donor molecules are completely ionized. Two $TTF^{+\cdot}$, one $DHCP^{2-}$ and one acetonitrile molecules are crystallographically independent.[12,18]

Two kinds of $TTF^{+\cdot}$ molecules (A, B) have different contributions in the crystal. Fig. 8a shows the crystal structure viewed along the *c*-axis. The TTF skeletons are cross hatched. The $TTF^{+\cdot}$ (A) molecules form a dimer with interplanar separation of 3.36 Å and overlap pattern depicted in Fig. 8b. The dimers form a segregated column along the [001] direction with a interdimer separation of 3.47 Å. Short S···S atomic contacts (dotted lines in Fig. 8) are observed within the column but not between the columns as shown in Fig. 8c, which is a view along the short axis of TTF. The solvent molecules separate the $TTF^{+\cdot}$ (A) segregated columns from the $TTF^{+\cdot}$ (B) molecules in the direction of the short axis of $TTF^{+\cdot}$ (A) molecule (Fig. 8a and 8b). Along the molecular long axis of $TTF^{+\cdot}$ molecule the segregated column is sandwiched by the bis(dicyanomethyl)methylide group (TCA1 part) linked to C4 of $DHCP^{2-}$ (Fig. 8b). The rest of $DHCP^{2-}$ (TCA2 part) contributes to the formation of an alternating stack with another kind of $TTF^{+\cdot}$ (B) molecules.

Fig. 8d shows an ADDA stack consisting of $DHCP^{2-}$···$TTF^{+\cdot}$ (B) ···$TTF^{+\cdot}$ (B)···$DHCP^{2-}$ tetrad with the interplanar distance of 3.45 Å ($TTF^{+\cdot}$ (B)···$DHCP^{2-}$) and 3.30 Å ($TTF^{+\cdot}$ (B)···$TTF^{+\cdot}$ (B)). Short N···S and N···H atomic contacts (3.01–3.26 Å *vs.* sum of van der Waals radii 3.35 Å for 5 kinds of N···S contacts, and 2.48–2.74 Å *vs.* 2.75 Å for 11 kinds of N···H contacts) exist between $TTF^{+\cdot}$ (B) and $DHCP^{2-}$ molecules as shown by dashed lines. We see the $DHCP^{2-}$ molecule modifies its conformation in order to make as many short N···S and N···H atomic contacts as possible to stabilize the lattice. The sequence of tetrads constructs an infinite double column of a DA stack along the *a*-axis as indicated by arrows in Fig. 8e.

3.5 Crystal and band structures of ET complexes

Density measurements reveal that both **ET1** and **ET2** have the same stoichiometry of $(ET)_4(DHCP)(THF)_x$ ($x \approx 2$), which requires a partial CT state for the ET molecules. Crystal-

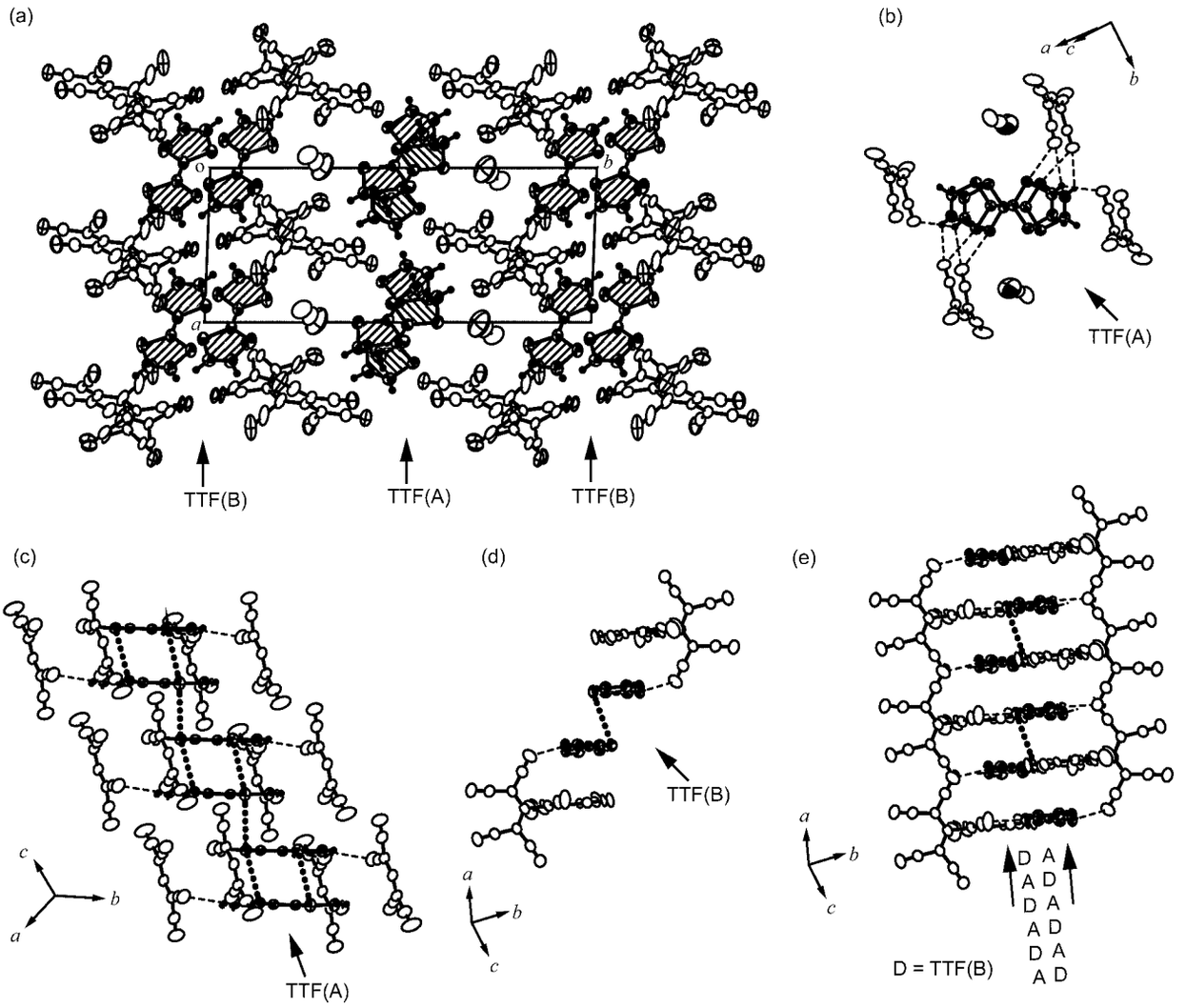

Fig. 8 Crystal structure of $(TTF)_2(DHCP)(CH_3CN)$ (**TTF**) (a) Viewed along the *c*-axis. $TTF^{+\cdot}$ (A) and $TTF^{+\cdot}$ (B) are hatched. (b) $TTF^{+\cdot}$ dimer in the $TTF^{+\cdot}$ (A) segregated column which is sandwiched by planes of terminal bis(dicyanomethyl)methylide groups (TCA1 part) linked to C4 of DHCP molecules. (c) Viewed along the short axis of TTF(A). (d) An ADDA tetrad composed of the dianion and TTF(B). (e) Two neighboring DA alternating stacks constructed of ADDA tetrads along the *a*-axis at $y=0$. Dotted and dashed lines represent atomic contacts of S···S (dotted line) or S···N and H···N (dashed line) shorter than the sum of van der Waals radii, respectively. In (b) and (c) only the TCA1 part linked to C4 of DHCP molecules are depicted for simplicity.

lographic data are summarized in Table 3. Although the ratios of the number of reflections to that of the parameters in the least-squares procedures are not sufficient in **ET1** and **ET2**, the final results are reliable to derive the band electronic and structural aspects. Both in **ET1** and **ET2**, the THF molecules show large temperature factors, which indicate the possible disorder in the crystals. Fig. 9 and 10 present the crystal structures of **ET1** and **ET2**, respectively.

Fig. 9a shows only ET molecules in the **ET1** sample. There are four crystallographically independent ET molecules (A–D). They form a face-to-face stacking with dimerization along the [102] direction (Fig. 9b). The interplanar spacing of ET molecules ranges from 3.67 to 3.82 Å. Ethylene conformations are eclipsed both in A and B molecules, while the ethylene groups of the C and D molecules are disordered. Short $S_{in}\cdots S_{out}$ and $S_{out}\cdots S_{out}$ atomic contacts are observed only along side-by-side direction, where S_{in} and S_{out} are sulfur atoms in the TTF moiety and outer six-membered rings, respectively. No $S_{in}\cdots S_{in}$, of which the HOMO coefficient is 2.8 times larger than that of S_{out}, was observed as common for the ET compounds. The packing mode (Fig. 9c, β''_{421})[23] is similar to that in $(ET)_4[M(CN)_4]H_2O$ (M = Ni, Pd, Pt) (β''_{421}).[24] The calculated band structure and density of states (DOS) are depicted in Fig. 11a. The Fermi level lies just between the first

Table 3 Crystallographic data of BEDT-TTF complexes of $DHCP^{2-}$

	$(BEDT\text{-}TTF)_4(DHCP)(THF)_x$ ($x\approx2$)	
	ET1	**ET2**
Formula	$C_{62}H_{48}N_8O_2S_{32}$	$C_{62}H_{48}N_8O_2S_{32}$
Formula weight	1963.23	1963.23
Crystal system	Triclinic	Triclinic
Space group	$P1$	$P\bar{1}$
a/Å	11.666(3)	15.365(7)
b/Å	19.620(4)	21.369(9)
c/Å	9.523(2)	12.961(5)
α/°	96.38(4)	99.92(3)
β/°	112.72(2)	105.22(5)
γ/°	89.35(3)	77.02(5)
V/Å^3	2001.1(9)	3972(3)
Z	1	2
μ(Mo-K$_\alpha$)/mm^{-1}	0.90	0.90
Temperature of data collection	Room temp.	Room temp.
No. of reflections measured	18324	7660
No. of independent reflections	9644	7109
R_{int}	0.1693	0.0102
No. of reflections used	6236	4946
$wR(F^2)$	0.1398	0.1880
R	0.0702	0.0603

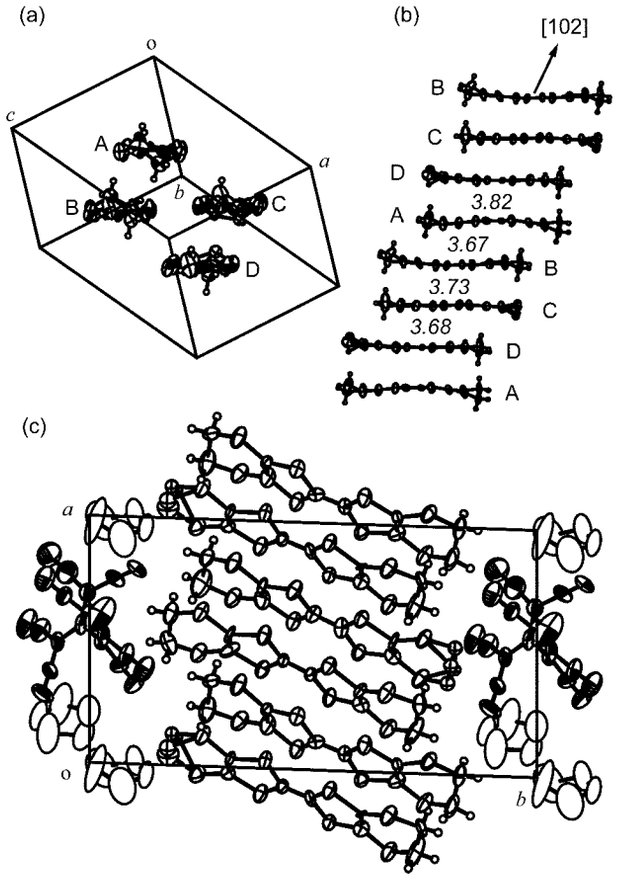

Fig. 9 Crystal structure of $(BEDT–TTF)_4(DHCP)(THF)_x$ ($x \approx 2$) (**ET1**). (a) Donor packing in unit cell. (b) View of the ET column along the molecular short axis, italic numbers between ET molecules indicate interplanar distances (Å). (c) A unit cell viewed along the *c*-axis.

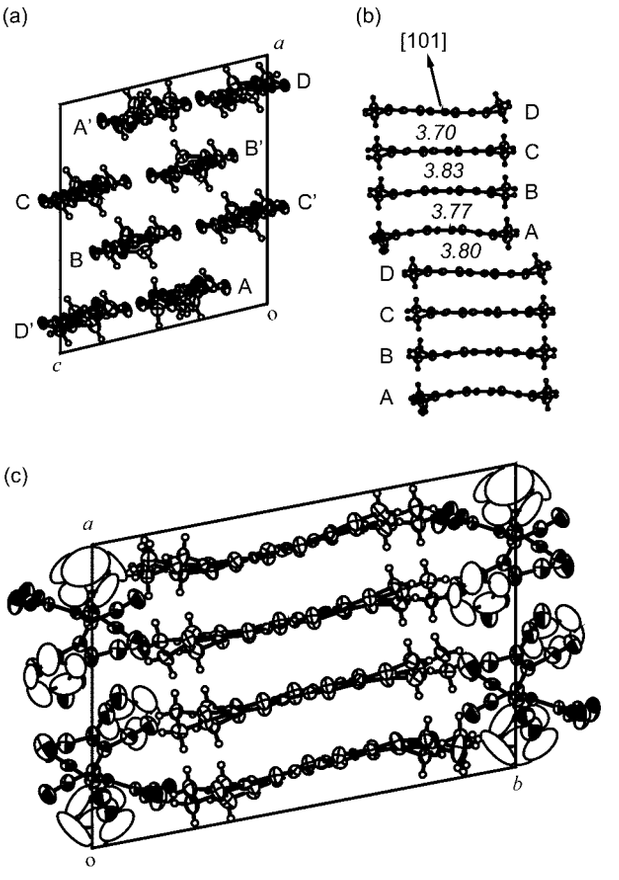

Fig. 10 Crystal structure of $(BEDT–TTF)_4(DHCP)(THF)_x$ ($x \approx 2$) (**ET2**). (a) Donor packing in unit cell viewed along the *b*-axis. (b) View of the ET column along the molecular short axis, italic numbers between ET molecules indicate interplaner distances (Å). (c) View along the *c*-axis.

and second HOMO bands and the band gap is estimated to be 26 meV. Therefore, as far as the band calculation is concerned, the **ET1** sample is concluded to be a narrow gap semiconductor. However as described in ref. 25, a semimetallic feature was also deduced by using different parameters in the band calculation. These results suggest that **ET1** is located on the border between a narrow gap semiconductor and a semimetal.

The ET molecules in **ET2** viewed along the *b*- and *c*-axes are presented in Fig. 10a and 10c, respectively. Four ET molecules (A–D) are crystallographically independent. They form tetrads and stack along the [101] direction with short $S_{in}\cdots S_{out}$ and $S_{out}\cdots S_{out}$ atomic contacts only along the side-by-side (*c*-axis) direction. The interplanar distances of the ET molecules range from 3.70 to 3.83 Å. The ethylene groups have eclipsed conformation except for the A molecule which has disordered ethylene group. The donor packing mode ($\beta''_{410\times2}$) is similar to those of $(ET)_2ClO_4(TCE)_{0.5}$ (β''_{412})[26] and $(ET)_4M(CN)_4$ (M = Ni, Pd, Pt) (β''_{411})[27] but the $\beta''_{410\times2}$-type has never been reported so far. The calculated band structure, DOS and Fermi surface are shown in Fig. 11b and 11c. Since the value of Z equals 2, eight HOMO orbitals of ET molecules construct the wide valence band of 0.93 eV. The calculated Fermi surface consists of both the electron and hole pockets. The metallic nature of the **ET2** sample is consistent with the presence of the Fermi surface.

Before describing the molecular structure of DHCP and the intermolecular atomic contacts between DHCP and ET molecules in **ET1** and **ET2**, their magnetic properties will be discussed.

3.6 EPR parameters of ET complexes

EPR measurements were performed on the samples of **ET1** and **ET2**, that exhibited the electric conductivity shown in Fig. 7a and 7b, respectively, with the external magnetic field almost parallel to the *b*-axis that is nearly parallel to the long molecular axis of the ET molecules. A Lorentzian signal with a nearly similar peak-to-peak line width (ΔH) of 3.5 mT (**ET1**) or 4.0 mT (**ET2**) is observed at RT. Fig. 12a and 12b present the temperature dependence of the EPR parameters of **ET1** and **ET2** samples, respectively. The main signal of the **ET1** sample is extinguished at around 50 K and a new signal due to defects appears at lower temperatures. In contrast to this, the signal for the **ET2** sample survived down to 1.8 K which is consistent with the metallic behavior of **ET2** in Fig. 7b.

The *g*-values at room temperature of 2.012 (**ET1**) and 2.013 (**ET2**) are in good accordance with the molecular *g*-value of $ET^{+\cdot}$ along the molecular long axis.[28] The *g*-values are almost temperature independent (2.0119–2.0126 for **ET1**, 2.0128–2.0137 for **ET2**).

The temperature dependencies of ΔH and relative intensity ($I(T)/I(300)$) exhibit characteristic features as follows.

For **ET1**, ΔH is constant in the highly conductive region and shows rapid narrowing at low temperatures (0.7 mT at 50 K). The intensity decreases with an inflection at *ca.* 200 K down to 50 K, below which almost nil intensity is detected. So the phase transition of **ET1** at around 180–200 K extinguishes both the mobile electrons and spins simultaneously. In accordance with this, an Arrhenius plot of the electrical resistivity and the spin susceptibility ($\chi_{spin} = CT^{-1}\exp(-\varepsilon_a/k_BT)$, k_B: Boltzmann constant) yields almost the same activation energies of 44 meV and 32 meV, respectively. The constant line width and the gradual decrease of intensity above 200 K is suggestive of a semiconductive nature. However, the temperature dependencies of the EPR intensity, the line width and electrical resistivity are very reminiscent to those observed for semimetallic

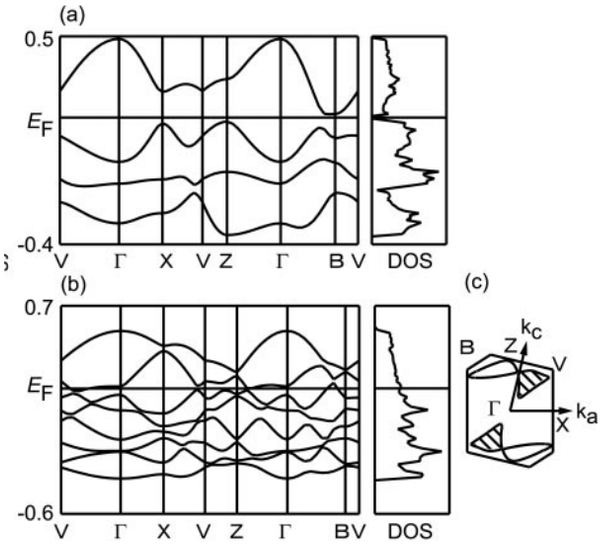

Fig. 11 Calculated band structure and density of states (DOS) of (BEDT–TTF)$_4$(DHCP) (THF)$_x$ ($x \approx 2$). (a) **ET1**. (b) **ET2**. (c) Fermi surface of **ET2**. Electron-like Fermi pockets are hatched.

$(ET)_4Pd(CN)_4$.[24] Therefore it is not yet convincing that **ET1** is a semimetal or a narrow-gap semiconductor above 200 K.

The EPR linewidth of **ET2** exhibits a monotonous and gradual decrease, at first, down to 150 K followed by a rapid decrease. This kind of temperature dependence of ΔH is compatible with the Elliott mechanism[29] and has often been observed in organic metals such as β-$(ET)_2X$ (X = I_3, IBr_2, AuI_2)[30] and β″-$(ET)_2X$ (X = $AuBr_2$, ICl_2).[31] Although these β- and β″-$(ET)_2X$ are metallic down to low temperatures, the temperature dependence of the spin susceptibility is remarkably different between them. The spin susceptibility of β-$(ET)_2X$ is insensitive to temperature in accordance with the Pauli paramagnetism. This is a characteristic feature for the metallic ET compounds with a large Fermi surface, the area of which is insensitive to temperature. On the other hand, the spin susceptibility of β″-$(ET)_2X$ is very dependent on the temperature because of the semimetallic Fermi surface with a small area. For such a semimetal, the density of state at the Fermi level is possibly very susceptible to temperature. Temperature dependence of the spin susceptibility of **ET2** in Fig. 12b is similar to that of β″-$(ET)_2X$. The intensity shows a continuous decrement down to 50 K, where the relative intensity is *ca.* 30% of that at RT. Below 50 K, the intensity shows an upturn. The upturn of the spin susceptibility is ascribed to a Curie impurity. Even after subtraction of the Curie impurity from the observed susceptibility, χ_{spin} still shows temperature dependent behavior

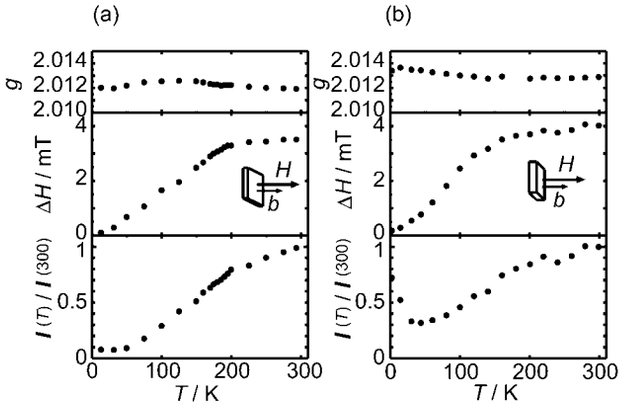

Fig. 12 Temperature dependence of EPR *g*-values, peak-to-peak line widths (ΔH) and spin susceptibilities (relative value, $I(T)/I(300\ K)$). (a): **ET1**. (b): **ET2**. The external magnetic field is parallel to the *b*-axis.

reminiscent to those of β″-$(ET)_2X$[31] and semimetallic $(ET)_4[Pt(CN)_4]H_2O$.[24]

Summarizing, the electrical conductivities and magnetic susceptibilities of **ET1** and **ET2** exhibited marked differences which have been explained by taking into account the band structures based on the packing of ET molecules in **ET1** and **ET2**. In the following we describe the molecular structure of DHCP and the donor–anion interactions, which are the main origins of the different packing of ET molecules and the resulting physical properties of **ET1** and **ET2**.

3.7 Molecular structure of DHCP and donor–anion interaction

The molecular structures of DHCP in **ET1** and **ET2** (Fig. 13) are different from one another. Their conformations are related to each other by a rotation at the C4–C5 bond, though the C4–C5 bonds of DHCP in **ET1** and **ET2** have double bond character (C4–C5 1.40(2) and 1.40(1) Å; C5–C12 1.47(1) and 1.43(2) Å, for **ET1** and **ET2**, respectively). The tetracyanoallyl group (TCA1 part) at C4 and the dicyanomethyl group at C5 are related in *cis*- and *trans*-conformations in **ET1** and **ET2**, respectively. The conformation of the DHCP molecule of **ET1** (Fig. 13a) is similar to that of the TEA salt (Fig. 5b) and is related to that of the TMA salt (Fig. 5a) by a rotation of the C1–C4 bond. As summarized in Table 2, the φ values are 65.8 and 53.6° for **ET1** and **ET2**, respectively. The ϕ values are 13.3 and 14.6° for **ET1** and 20.2 and 17.7° for **ET2** for the dicyanomethyl groups N1≡C7–C2–C8≡N2 and N3≡C9–C3–C10≡N4, respectively. **ET2** has the smallest φ value and the largest ϕ values of all the DHCP molecule studied here. In summary it is said that the φ value ranges from 53.6° (**ET2**) to 69.8° (**TTF**) and the ϕ value from 0.9° (**TTF**) to 20.2° (**ET2**) indicating the highly flexible nature of the molecular shape of DHCP.

All the N atoms of DHCP have short atomic contacts with S_{out} atoms or H atoms but not with S_{in} atoms of ET molecules as shown in Fig. 14. Two kinds of ET complexes are harvested with the anion in both conformations (*cis*- or *trans*-) with as many atomic contacts as possible between constituent molecules.

Not very many N···S contacts (dotted lines in Fig. 14) exist (two kinds for **ET1** and three kinds for **ET2**) compared to those in **TTF** (5 kinds). A considerably short N···S contact is observed in **ET1** (3.05 Å) compared to that in **ET2** (3.16 Å). However, since the HOMO coefficient of S_{out} of ET is much smaller than that of S of TTF, the efficiency of the N···S contacts for lattice formation seems to be less in the ET complexes than the TTF complex.

Even though the position of H atoms contains some ambiguity due to the disorder of the ethyl groups of ET, numbers of short N···H contacts (dashed lines in Fig. 14) are found where the C–H bond length is assumed to be 0.96 Å to avoid the overestimation of the intermolecular atomic contacts. It should be emphasized that all the N atoms of DHCP contribute to the formation of the N···H contacts. Nine kinds

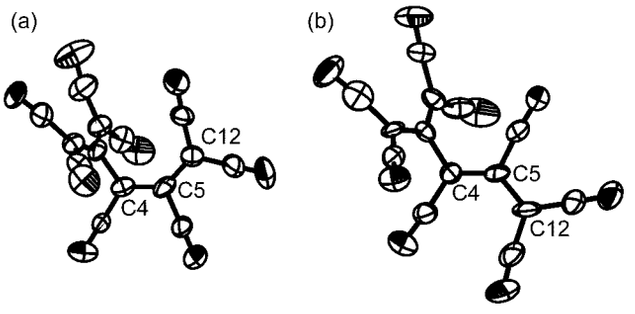

Fig. 13 Molecular structures of DHCP in (BEDT–TTF)$_4$(DHCP)(THF)$_x$ ($x \approx 2$). (a) **ET1** and (b) **ET2**.

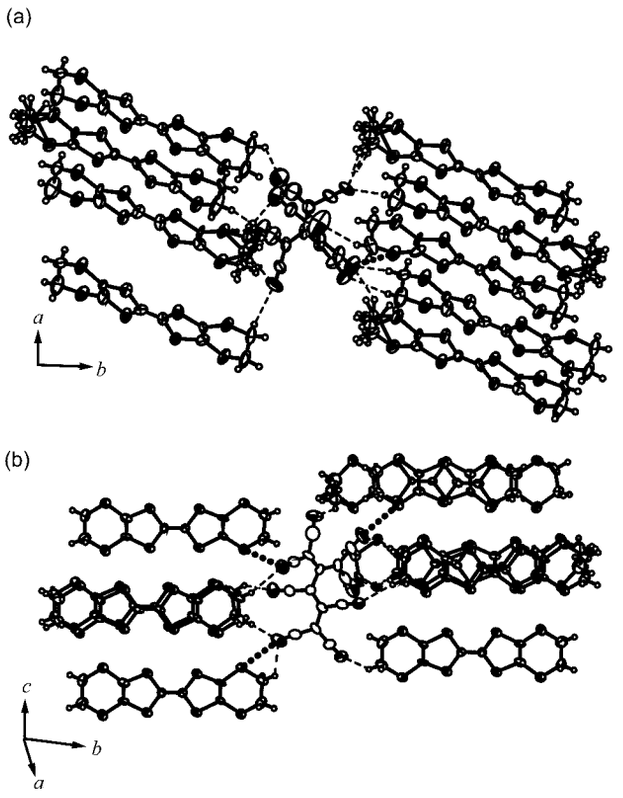

Fig. 14 Significantly short N···S (dotted line) and N···H (dashed line) atomic contacts between DHCP and BEDT–TTF molecules in $(BEDT–TTF)_4(DHCP)(THF)_x$ ($x \approx 2$). (a) **ET1** and (b) **ET2**. The BEDT–TTF molecules which do not have short N···S and N···H atomic contacts are omitted for clarity.

of H atoms form such contacts with distances ranging from 2.21(4) to 2.74(3) Å for **ET1** while eight kinds of H atoms are found in **ET2**. The shortest contact in **ET2** is estimated at 2.53(2) Å while nearly half the number of N···H contacts in **ET1** (2.21–2.52 Å) are shorter than that. This observation implies that the ET molecules are located at a closer proximity to the DHCP in **ET1** than **ET2**, though the number of disordered ethyl groups is greater in **ET1** (two disordered ethyl groups out of four ET molecules) than in **ET2** (one such ethyl group out of four ET).

The calculated density of the crystals (d_{calc}) implies that the constituent molecules are more tightly packed in **ET2** ($d_{cals} = 1.642$ g cm^{-3}) than **ET1** ($d_{calc} = 1.629$ g cm^{-3}). Consequently, it is deduced that the ET molecules in **ET1** are loosely packed in the donor layer compared to the dense packing in **ET2**. These deductions partly imply the occurrence of two different β″-type packings of ET molecules and their different physical properties as described.

The area of anion layer per donor is important in order to determine the packing motifs of the ET molecules and hence the band energy dispersion including the shape of the Fermi surface and the dimensionality. When the area of anion expands, the number of "dislocations" in the ET column is increased in general. Here "dislocation" means a large slip of the ET molecule along the molecular long axis in the column.[23] In typical β″-type salts, the large anion area (100–105 Å^2/four ET molecules) makes a β''_{42}-type or β''_{21}-type which has two dislocations per four ET molecules. The small anion area (95–100 Å^2/four ET molecules) makes β''_{41}-type which has one dislocation per four ET molecules. In our case, the large area 102.5 Å^2/four ET molecules in **ET1** and the small area 96.1 Å^2/four ET molecules in **ET2** results in the formation of β''_{42}-type and β''_{41}-type packing, respectively. Furthermore, the larger area of anion in **ET1** agrees with the looser packing of the ET molecules, which was also observed in the above mentioned atomic contacts and the crystal density.

4 Conclusion and summary

2-Dicyanomethylene-1,1,3,4,5,5-hexacyanopentadiene (DHCP, **4**) dianion molecule, which has previously been reported as 2,3-bis(dicyanomethyl)-1,1,4,4-tetracyanopentadiene, is identified directly by structural analysis and its formation process from hexacyanobutadiene is deduced based on its molecular structure. The DHCP dianion molecule is able to accommodate its conformation depending on the size, shape of the counter cation molecules and surrounding circumstances in the solid. Seven conductive solid charge transfer complexes are prepared with TTF derivatives as electron donors. **BO** is metallic down to 4.2 K. ET affords two metallic complexes, one of which (**ET1**) shows a metal–insulator transition at 180 K and the other (**ET2**) remains metallic down to 1.3 K. The spin susceptibility in the metallic region of both **ET1** and **ET2** is sensitive to temperature, suggesting a semimetallic nature. The possibility of a narrow-gap semiconductor is not excluded for **ET1**. The conformational flexibility of the DHCP dianion and short atomic contacts between the N atoms of DHCP and H or S atoms of donor molecules are the origins for the unique packing of component molecules in the **TTF** complex and metallic polymorphs with ET. This finding illustrates that large and flexible organic anions are useful for exploring novel molecular conductors and may also contribute to new functional materials.

Acknowledgements

The authors acknowledge Professors T. Momose and T. Shida for EPR spectrometry. Also we thank Professor T. Mori for the advice on altering the programs for band calculation. We thank Dr N. Ueba for a kind gift of BTPDT–TTF and BOPDT–TTF. This work was in part supported by a Grant-in-Aid for Scientific Research from the Ministry of Education, Science, Sports, and Culture, Japan, a Grant for CREST (Core Research for Evolutional Science and Technology) of Japan Science and Technology Corporation (JST) and a fund for "Research for the Future" from the Japan Society for Promotion of Science.

References

1 (*a*) T. L. Cairns, R. A. Carboni, D. D. Coffman, V. A. Engelhardt, R. E. Heckert, E. L. Little, E. G. McGeer, B. C. McKusick, W. J. Middleton, R. M. Scribner, C. W. Theobald and H. E. Winberg, *J. Am. Chem. Soc.*, 1958, **80**, 2775; (*b*) D. N. Dhar, *Chem. Rev.*, 1967, **67**, 611; (*c*) A. J. Fatiadi, *Synthesis*, 1986, 249; (*d*) A. J. Fatiadi, *Synthesis*, 1986, 749; (*e*) A. J. Fatiadi, *Synthesis*, 1987, 959.

2 (*a*) B. C. McKusick, R. E. Heckert, T. L. Cairns, D. D. Coffman and H. F. Mower, *J. Am. Chem. Soc.*, 1958, **80**, 2806; (*b*) J. R. Roland and B. C. McKusick, *J. Am. Chem. Soc.*, 1961, **83**, 1652.

3 (*a*) T. Miura and Y. Masaki, *Tetrahedron*, 1995, **51**, 10477; (*b*) Y. Masaki, T. Miura and M. Ochiai, *Bull. Chem. Soc. Jpn.*, 1996, **69**, 195.

4 (*a*) J. F. Nicoud and R. J. Twieg, *Nonlinear Optical Properties of Organic Molecules and Crystals*, ed. D. S. Chemla and J. Zyss, Academic Press, Orlando, Tokyo, 1987, vol. 1, p. 227; (*b*) M. Matsuoka, T. Kitao and K. Nakatsu, *Nonlinear Optics of Organics and Semiconductors*, ed. T. Kobayashi, Springer-Verlag, Berlin, Tokyo, 1989, p. 228; (*c*) T. Gotoh, K. Kondoh, K. Egawa and K. Kubodera, *J. Opt. Soc. Am. B*, 1989, **6**, 703; (*d*) Q. Gong, Z. Xia, Y. H. Zou, X. Meng, L. Wei and F. Li, *Appl. Phys. Lett.*, 1991, **59**, 381.

5 (*a*) W. R. Hertler, W. L. Mahler, R. Melby, J. S. Miller, R. E. Putscher and O. W. Webster, *Mol. Cryst. Liq. Cryst.*, 1989, **171**, 205 and references cited therein ; (*b*) F. Wudl and E. W. Southwick, *J. Chem. Soc., Chem. Commun.*, 1974, 254;

(*b*) R. C. Wheland and J. L. Gillson, *J. Am. Chem. Soc.*, 1976, **98**, 3916.
6 (*a*) J. S. Miller, A. J. Epstein and W. M. Reiff, *Acc. Chem. Res.*, 1988, **21**, 114; (*b*) J. S. Miller, A. J. Epstein and W. M. Reiff, *Chem. Rev.*, 1988, **88**, 201; (*c*) J. S. Miller and A. J. Epstein, *Angew. Chem., Int. Ed. Engl.*, 1994, **33**, 385; (*d*) J. S. Miller and A. J. Epstein, *Chem. Commun.*, 1998, 1319.
7 (*a*) W. Kaim and M. Moscheroshc, *Coord. Chem. Rev.*, 1994, **129**, 157; (*b*) K. R. Dunbar, *Angew. Chem., Int. Ed. Engl.*, 1996, **35**, 1659; (*c*) L. Jäger, C. Tretner, H. Hartung and M. Biedermann, *Chem. Ber. Recl.*, 1997, **130**, 1007; (*d*) S. Duclos, F. Conan, S. Triki, Y. Le Mest, M. L. Gonzalez and J. S. Pala, *Polyhedron*, 1999, **18**, 1935; (*e*) S. Triki, J. S. Pala, M. Decoster, P. Molinie and L. Toupet, *Angew. Chem., Int. Ed.*, 1999, **38**, 113.
8 (*a*) A. M. Kini, U. Geiser, H. H. Wang, K. D. Carlson, J. M. Williams, W. K. Kwok, K. G. van Devoort, J. E. Thompson, D. L. Stupka, D. Jung and M.-H. Whangbo, *Inorg. Chem.*, 1990, **29**, 2555; (*b*) J. M. Williams, A. M. Kini, H. H. Wang, K. D. Carlson, U. Geiser, L. K. Montgomery, G. J. Pyrka, D. M. Watkins, J. M. Kommers, S. J. Boryshuk, V. S. Crouch, W. K. Kwok, J. E. Schirber, D. L. Overmyer, D. Jung and M.-H. Whangbo, *Inorg. Chem.*, 1990, **29**, 3272; (*c*) T. Komatsu, T. Nakamura, N. Matsukawa, H. Yamochi, G. Saito, H. Ito, T. Ishiguro, M. Kusunoki and K. Sakaguchi, *Solid State Commun.*, 1991, **80**, 843; (*d*) H. Yamochi, T. Komatsu, N. Matsukawa, G. Saito, M. Kusunoki and K. Sakaguchi, *J. Am. Chem. Soc.*, 1993, **115**, 11319.
9 (*a*) M. Kurmoo and C. J. Kepert, *New J. Chem.*, 1998, **22**, 1515; (*b*) J. L. Manson, C. R. Kmety, Q. Huang, J. W. Lynn, G. M. Bendele, S. Pagola, P. W. Stephens, L. M. Liable-Sands, A. L. Rheingold, A. J. Epstein and J. S. Miller, *Chem. Mater.*, 1998, **10**, 2552; (*c*) H. Hoshino, K. Iida, T. Kawamoto and T. Mori, *Inorg. Chem.*, 1999, **38**, 4229; (*d*) J. L. Manson, A. M. Arif and J. S. Miller, *J. Mater. Chem.*, 1999, **9**, 979; (*e*) S. R. Batten, B. F. Hoskins, B. Moubaraki, K. S. Murray and R. Robson, *J. Chem. Soc., Dalton Trans.*, 1999, 2977; (*f*) S. R. Batten, P. Jensen, C. J. Kepert, M. Kurmoo, B. Moubaraki, K. S. Murray and D. J. Price, *J. Chem. Soc., Dalton Trans.*, 1999, 2987.
10 O. W. Webster, *J. Am. Chem. Soc.*, 1964, **86**, 2898.
11 (*a*) G. Saito, H. Hayashi, T. Enoki and H. Inokuchi, *Mol. Cryst. Liq. Cryst.*, 1985, **120**, 341; (*b*) C. Katayama, M. Honda, H. Kumagai, J. Tanaka, G. Saito and H. Inokuchi, *Bull. Chem. Soc. Jpn.*, 1985, **58**, 2272; (*c*) H. Yamochi, G. Saito, T. Sugano, M. Kinoshita, C. Katamaya and J. Tanaka, *Chem. Lett.*, 1986, 1303; (*d*) H. Yamochi, T. Tsuji, G. Saito, T. Suzuki, T. Miyashi and C. Kabuto, *Synth. Met.*, 1988, **27**, A479; (*e*) H. Yamochi, T. Nakamura, G. Saito, T. Kikuchi, S. Sato, K. Nozawa, M. Kinoshita, T. Sugano and F. Wudl, *Synth. Met.*, 1991, **41–43**, 1741; (*f*) H. Yamochi, C. Tada, S. Sekizaki, G. Saito, M. Kusunoki and K. Sakaguchi, *Mol. Cryst. Liq. Cryst.*, 1996, **284**, 379; (*g*) H. Yamochi, K. Tsutsumi, T. Kawasaki and G. Saito, *Mater. Res. Soc. Symp. Proc.*, 1998, **488**, 641; (*h*) S. Sekizaki, H. Yamochi and G. Saito, *Synth. Met.*, 1999, **102**, 1711; (*i*) K. Nishimura, T. Kondo, O. O. Drozdova, H. Yamochi and G. Saito, *J. Mater. Chem.*, 2000, **10**, 911.
12 H. Yamochi, A. Konsha, G. Saito, K. Matsumoto, M. Kusunoki and K. Sakaguchi, *Mol. Cryst. Liq. Cryst.*, in press.
13 Properties of $(TEA)_2$**4** [in brackets the reported values for $(TEA)_2$**3** in reference 10 are indicated]: mp. 209–213 °C [205–211]; IR (KBr, cm^{-1}) 2190(s), 1454(s), 1299(w), 1240(w) [2193(s), 1453(s), 1297(w), 1239(w)]; UV–Vis (acetonitrile) 323 nm ($\varepsilon = 20230$), 420 (20290) [328 (20100), 420 (20100)].
14 Cyclic voltammetric measurements were performed in a 0.1 mol L^{-1} solution of (tetra-*n*-butylammonium)BF_4 in acetonitrile with Pt working electrodes, scanning speed of 200 mV s^{-1} at 24 °C.
15 Abbreviations for chemicals in the text: TTF, tetrathiafulvalene; BEDT–TTF or ET, 3,4:3′,4′-bis(ethylenedithio)tetrathiafulvalene; BEDO–TTF or BO, 3,4:3′,4′-bis(ethylenedioxy)tetrathiafulvalene; EDT–TTF, 3,4-ethylenedithiotetrathiafulvalene; BVDT–TTF, 3,4:3′,4′-bis(vinylenedithio)tetrathiafulvalene; BPDT–TTF, 3,4:3′,4′-bis(propylenedithio)tetrathiafulvalene, BTPDT–TTF, 3,4:3′,4′-bis(thiapropylenedithio)tetrathiafulvalene; BOPDT–TTF, 3,4:3′,4′-bis(oxapropylenedithio)tetrathiafulvalene; BMDT-TTF, 3,4:3′,4′-bis(methylenedithio)tetrathiafulvalene; HMTTF, 3,4:3′,4′-hexamethylenetetrathiafulvalene; TMTTF, 3,4:3′,4′-tetramethyltetrathiafulvalene; TMTSF, 3,4:3′,4′-tetramethyltetraselenafulvalene; OMTTF, 3,4:3′,4′-octamethylenetetrathiafulvalene; TMB, *N*,*N*,*N*′,*N*′-tetramethylbenzidine.
16 (*a*) A. Altomare, G. Cascarano, C. Giacovazzo, A. Guagliardi, M. C. Burla, G. Polidori and M. Camalli, *SIR92*, adapted by S. Mackay for Crystan-GM, MAC Science Co. Ltd., 1995; (*b*) G. M. Sheldrick SHELXL-93, University of Göttingen, 1993.
17 T. Mori, A. Kobayashi, Y. Sasaki, H. Kobayashi, G. Saito and H. Inokuchi, *Bull. Chem. Soc. Jpn.*, 1984, **57**, 627.
18 In this paper, more atoms at the disordered part of DHCP were taken into consideration than in reference 12.
19 (*a*) T. J. Johnson, K. W. Hipps and R. D. Willett, *J. Phys. Chem.*, 1988, **92**, 6892; (*b*) M. L. Yates, A. M. Arif, J. L. Manson, B. A. Kalm, B. Burkhart and J. S. Miller, *Inorg. Chem.*, 1998, **37**, 840.
20 (*a*) S. Horiuchi, H. Yamochi, G. Saito, K. Sakaguchi and M. Kusunoki, *J. Am. Chem. Soc.*, 1996, **118**, 8604; (*b*) T. Senga, K. Kamoshida, L. A. Kushch, G. Saito, T. Inamoto and I. Ono, *Mol. Cryst. Liq. Cryst.*, 1997, **296**, 97; (*c*) O. O. Drozdova, V. N. Semkin, R. M. Vlasova, N. D. Kushch and E. B. Yagubskii, *Synth. Met.*, 1994, **64**, 17; (*d*) T. Hasegawa, S. Kagoshima, T. Mochida, S. Sugiura and Y. Iwasa, *Solid State Commun.*, 1997, **103**, 489.
21 (*a*) T. Osada, R. Yagi, A. Kawasumi, S. Kagoshima, N. Miura, M. Oshima and G. Saito, *Phys. Rev. B*, 1990, **41**, 5428; (*b*) H. Taniguchi, H. Sato, Y. Nakazawa and K. Kanoda, *Phys. Rev. B*, 1996, **53**, R8879; (*c*) H. Taniguchi, Y. Nakazawa and K. Kanoda, *Phys. Rev. B*, 1998, **57**, 3623.
22 For reviews: (*a*) P. A. Lee and T. V. Ramakrishnan, *Rev. Mod. Phys.*, 1985, **57**, 287; (*b*) G. Bergmann, *Phys. Rep.*, 1984, **107**, 1.
23 T. Mori, *Bull. Chem. Soc. Jpn.*, 1998, **71**, 2509.
24 (*a*) H. Mori, I. Hirabayashi, S. Tanaka, T. Mori, Y. Maruyama and H. Inokuchi, *Solid State Commun.*, 1991, **80**, 411; (*b*) T. Mori, R. Kato, Y. Maruyama, H. Inokuchi, H. Mori, I. Hirabayashi and S. Tanaka, *Solid State Commun.*, 1992, **82**, 177.
25 By employing double-ζ parameters and excluding 3d orbitals of sulfur, the band structure produces a semimetallic feature with small hole pocket at X-point and small electron pocket at B-point. The double-ζ parameters were taken from M.-H. Whangbo, J. M. Williams, P. C. W. Leung, M. A. Beno, T. J. Emge and H. H. Wang, *Inorg. Chem.*, 1985, **24**, 3500 The result is provided as supporting information(Fig. S5).
26 H. Kobayashi, A. Kobayashi, Y. Sasaki, G. Saito and H. Inokuchi, *J. Am. Chem. Soc.*, 1983, **105**, 297.
27 (*a*) L. Ouahab, J. Padiou, D. Grandjean, C. Garrigou-Lagrange, P. Delhaes and M. Bencharif, *J. Chem. Soc., Chem. Commun.*, 1989, 1038; (*b*) M. Tanaka, H. Takeuchi, A. Kawamoto, J. Tanaka, T. Enoki, K. Suzuki, K. Imaeda and H. Inokuchi, *The Physics and Chemistry of Organic Superconductors*, ed. G. Saito and S. Kagoshima, Springer-Verlag, Berlin, Tokyo, 1990, p. 298; (*c*) T. Mori and H. Inokuchi, *Chem. Lett.*, 1987, 1657.
28 T. Sugano, G. Saito and M. Kinoshita, *Phys. Rev. B*, 1986, **34**, 117.
29 R. J. Elliott, *Phys. Rev.*, 1954, **96**, 266.
30 (*a*) E. L. Venturini, L. J. Azevedo, J. E. Schirber, J. M. Williams and H. H. Wang, *Phys. Rev. B*, 1985, **32**, 2819; (*b*) D. R. Talham, M. Kurmoo, P. Day, D. S. Obertelli, I. D. Parker and R. H. Friend, *J. Phys. C*, 1986, **19**, L383; (*c*) B. Rothaemel, L. Forro, J. R. Cooper, J. S. Schilling, M. Weger, P. Bele, H. Brunner, D. Schweitzer and H. J. Keller, *Phys. Rev. B*, 1986, **34**, 704; (*d*) E. L. Venturini, J. E. Schirber, H. H. Wang and J. M. Williams, *Synth. Met.*, 1988, **27**, A243.
31 (*a*) M. Kurmoo, D. R. Talham, P. Day, I. D. Parker, R. H. Friend, A. M. Stringer and J. A. K. Howard, *Solid State Commun.*, 1987, **61**, 459; (*b*) A. Ugawa, Y. Okawa, K. Yakushi, H. Kuroda, A. Kawamoto, J. Tanaka, M. Tanaka, Y. Nogami, S. Kagoshima, K. Murata and T. Ishiguro, *Synth. Met.*, 1988, **27**, A407.